Research Article

Yuan Xie*, Yuanhua He, Xiantao Chen, Daqin Bu, Xiaolong He, Maoyong Zhi, and Mingwu Wang*

Relationship between mechano-bactericidal activity and nanoblades density on chemically strengthened glass

https://doi.org/10.1515/ntrev-2022-0008
received May 28, 2021; accepted October 21, 2021

Abstract: Establishing the correlation between the topography and the bactericidal performance is the key to improve the mechano-bactericidal activity. However, due to the complexity of the mechano-bactericidal mechanism, the correlation between density and bactericidal performance is still not clear. Based on this, a series of nanoblades (NBs) with various density but similar thickness and height were prepared on the chemically strengthened glass (CSG) substrate by a simple alkaline etching method. The mechano-bactericidal properties of NBs on CSG (NBs@CSG) surfaces exposed to *Escherichia coli* were evaluated. The results show that with the NB density increasing, the mechano-bactericidal performance of the surface increased first and then decreased. Besides, the bactericidal performance of NBs@CSG is not affected after four consecutive ultrasonic cleaning bactericidal experiments. This article can provide guidance for the design of the new generation of mechano-bactericidal surfaces. In addition, this technology is expected to be applied to the civil aviation cabin window lining.

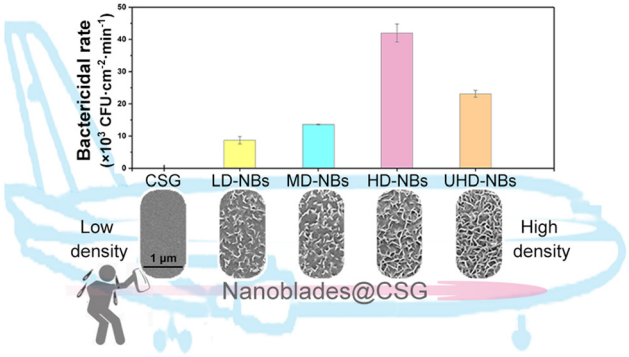

Graphical abstract: Topography and mechano-bactericidal performance of nanoblades (NBs) with different densities on the chemically strengthened glass for civil aircraft portholes. Low-density NBs, medium-density NBs, high-density NBs, and ultra-high density NBs.

Keywords: nanoblades, mechano-bactericidal activity, chemically strengthened glass, surface topography, alkaline etching

1 Introduction

The convenient and fast air transportation has become an important way for the spread of infectious microorganisms, allowing pathogens to spread over long distances. So the demand for the prevention and control of pathogenic microorganisms in cabins has risen to a new height [1]. Traditional cabin disinfection is time-consuming and laborious [2], it is very necessary to find a new technology to prevent and control the microorganisms in cabins quickly and efficiently [3]. Previous studies have shown that mechano-bactericidal has the above advantages [4], and its bactericidal performance is better than other surface treatment methods [5,6] (for example, quaternary ammonium salt [7] and nano heavy metal [8] disintegrate cell membranes by the chemical activity, antibiotics inhibit the synthesis of proteins and nucleic acids [9]). However,

* **Corresponding author: Yuan Xie,** College of Civil Aviation Safety Engineering, Civil Aircraft Fire Science and Safety Engineering Key Laboratory of Sichuan Province, Civil Aviation Flight University of China, Guanghan, Sichuan 618307, China, e-mail: cris_xy@126.com
* **Corresponding author: Mingwu Wang,** College of Civil Aviation Safety Engineering, Civil Aircraft Fire Science and Safety Engineering Key Laboratory of Sichuan Province, Civil Aviation Flight University of China, Guanghan, Sichuan 618307, China, e-mail: 1164638633@qq.com
Yuanhua He, Xiantao Chen, Daqin Bu, Maoyong Zhi: College of Civil Aviation Safety Engineering, Civil Aircraft Fire Science and Safety Engineering Key Laboratory of Sichuan Province, Civil Aviation Flight University of China, Guanghan, Sichuan 618307, China
Xiaolong He: National Laboratory of Biomacromolecules, Institute of Biophysics, Chinese Academy of Sciences, Beijing 100101, China

due to the complexity of the mechano-bactericidal action [10], the relationship between the bactericidal performance and topography is still not clear [11,12]. The basic research on correlation is of great value to the application of mechano-bactericidal method such as reduce labor costs [13,14].

As a large class of typical pathogenic microorganism, bacteria are ubiquitous in the cabin environment. It can realize the initial adhesion [15], proliferation [15], biofilm formation [16], and final migration [17] on the surface in a short time [18]. Each of the processes can cause the spread of bacteria [19,20] that infect a person through skin contact or breathing [21]. Passenger cabins are densely populated and relatively airtight places. Although cabins are equipped with filtration systems, it still cannot effectively prevent the people on board from being infected [2,22]. In particular, the surface of high-frequency touched such as chemically strengthened glass (CSG) of cabin window is easily contaminated with bacteria. Inhibiting or preventing the bacteria from replicating on such surface is the key to disease prevention and control [23]. At present, chlorine-containing and quaternary ammonium salt disinfectants are generally used for cabin disinfection [24]. However, these chemical treatment methods may not be durable, and the residual chemicals may remain on the surface and cause potential toxicity and irritation [25]. The limitation of the chemical treatment methods has caused that a complete cleaning of the cabin must be implemented after each flight, which would cost a lot of manpower to disinfect the inner face and significantly extend waiting time for boarding [3].

Since Ivanova *et al.* first discovered the nanopillar structure based on "mechano-bactericidal activity" from the insect surface [26,27], this method is expected to become the next generation of surface sterilization treatment [28–32]. The mechano-bactericidal activity is realized by the interaction between the nanoscale array structure on the surface and the bacterial cell, which destroys the integrity of the cell. The bactericidal performance does not depend on the chemical properties of the surface, so it has the advantage of not producing secondary contamination and drug-resistant bacteria [12,33]. The mechanical bactericidal performance is affected by many surface characteristic factors, such as geometry [34,35], size [36,37], height [38], pillar elasticity [5], aspect-ratio [38–40], surface irregularity [30,33], and substrate chemistry [41]. The results show that higher aspect ratio and lower tip diameter can improve the surface mechano-bactericidal activity by imposing more stress on the cells. However, due to the diversity of topography parameters and the complexity of the biocide mechanism, there is no accurate conclusion about the effect of the density of the bactericidal nano units on the mechano-bactericidal performance [11]. In our previous studies, a series of bactericidal Zn–Al LDHs nanoblades (NBs) were grown, the results show that the low tip-width and high-density NBs (HD-NBs) have higher bactericidal activity [42]. We found that the mechano-bactericidal performance was mainly affected by the tip-width of the bactericidal unit, and the lower top diameter could exert stronger force on the bacterial cell wall and destroy the cell integrity faster. Therefore, it is an effective method to improve the bactericidal performance by reducing the tip diameter of bactericidal units [43]. In addition, the increase of stress caused by different heights can also improve the bactericidal performance [6].

In particular, the density of the mechano-bactericidal unit (nanopillar, NBs) not only affects the number of bactericidal units on the substrate surface, but also determines the number of bactericidal units that single bacteria cells can contact, which is also an important factor affecting the mechano-bactericidal activity. However, it is not clear that the bactericidal rate increases infinitely as the density of NBs increases. Therefore, it is necessary to explore the "optimal density" of bactericidal NBs.

At present, the preparation of bionic bactericidal nanostructures mainly includes hydrothermal method [4,44], nanoimprint lithography [45], reactive-ion beam etching [26,46], chemical vapor deposition [40], and liquid-phase exfoliation [47]. However, for amorphous substrates (such as glass), it is difficult to grow firmly bonded nanostructures directly [48,49]. Although the lattice mismatch between array units and the substrate can be reduced by preforming a seed layer as a buffer [50,51], the additional process will greatly reduce the efficiency. The etching method can solve the above problems well [52]. The alkaline etching method of building nanostructure on the surface of CSG substrate can be realized.

In this study, we investigated the correlation between the density of NBs and their bactericidal properties. Aiming at the above bactericidal problems, the CSG substrates that have a series of NBs with similar thickness, length, height, and significantly different densities were etched by alkaline etching method, named low-density NBs (LD-NBs), medium-density NBs (MD-NBs), HD-NBs, and ultra-high-density NBs (UHD-NBs). The topography parameters and bactericidal performance of each sample were analyzed by scanning electron microscopic (SEM) images and sticking membrane method separately. And then the influence of NB density on bactericidal activity was explored, which can provide effective guidance for the design of efficient mechano-bactericidal nanostructures on civil aircraft portholes. We expect to prepare a simple, effective, efficient, and long-term bactericidal NB structure on the CSG substrate,

Table 1: The composition of CSG

	SiO_2	Na_2O	K_2O	CaO	Al_2O_3	MgO	Others
Weight percentage (%)	70.32	15.86	2.12	3.85	4.37	3.28	0.20

to realize the saving of manual disinfection labor, which is expected to be applied in the civil aviation field.

2 Experimental

2.1 Materials

CSG sheet 3 cm × 4 cm × 0.15 mm, medical disinfectant alcohol, pure ethanol, and potassium hydroxide (KOH) were purchased from Chang Zheng Chemicals Co., Ltd (Chengdu). All the chemicals used in this study were analytically pure. The etching solution was prepared with deionized water. The chemical composition of the original CSG surface is shown in Table 1.

2.2 Preparation of NBs by KOH etching

The cleaned CSG sheet was placed in 50 mL etching solution in a 100 mL teflon container, which was sealed by the stainless-steel reactor at 95°C. The 0.1 mol L^{-1} KOH was utilized as etching solution. To prepare a series of NBs, the etching time was controlled in 1, 2, 3, and 4 h. After etching, the products were cooled at room temperature, then the etched-CSG was cleaned by ionized water and dried in room temperature. Then each sample was cut to the appropriate size before use. The optical pictures of each etched-CSG sample are shown in Figure 1. There is no obvious difference in the appearance of the etched samples.

2.3 Characterization

To characterize the surface topographies of CSG and etched CSG, field emission scanning electron microscopy (FE-SEM, JEOL, JSM-7001F) was used at a voltage of 10 kV. Due to the poor conductivity of each sample, it is necessary to spray gold (10 mA, 70 s) before FE-SEM observation to ensure the observation effect. The Image J software was used to calculate the NB density. Steps are as follows: five 1 μm^2 areas were randomly selected in the SEM image of a sample. The topography parameters of the NBs in each area were counted respectively, and the average density was finally calculated. The composition of the samples was measured by energy dispersive spectrometer (EDS, Horiba 7021-H).

2.4 Bactericidal performance of NBs@CSG

To evaluate the bactericidal properties of the NBs@CSG against bacteria, the sticking membrane method referring to the Japanese Industrial Standard (JIS Z 2801) was used [53]. Each CSG sheet was assembled into a test device with a cavity of 1 cm × 1 cm × 0.12 cm, and the test surface constitute the under inner surface of the cavity. Before the bactericidal experiment, the whole device was immersed into disinfection alcohol for 1 min, and then transferred to the effective area of the clean bench (Shanghai Shu Li Instruments Co., Ltd, SW-CJ-1F) for drying. The *Escherichia coli* strain (*E. coli* ATCC 25922) was selected as the model strain in the experiment. The *E. coli* strain was successively activated and multiplied in a nutrient broth medium at 38°C for 3 h, and then the bacterial suspension was diluted to the standard concentration (5.0×10^6 CFU mL^{-1}) by sterilized normal saline. About 100 µL *E. coli* standard bacterial suspensions were carefully dropped into the cave of the test device and incubated at 37°C for 10 min. To avoid the influence of bacteria movement on the bactericidal properties of the surface [54], all droplets were added at a distance of

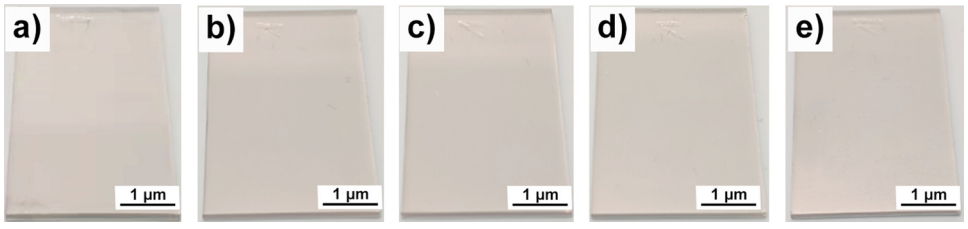

Figure 1: Optical pictures of CSG and NBs@CSG sheets: (a) CSG original sample; etched-CSG after etching for different time: (b) 1 h, (c) 2 h, (d) 3 h, and (e) 4 h.

0.5 cm from the CSG sample. To count the number of live bacteria on the surface, each sample was thoroughly washed with sterilized physiological saline (10 mL). After the eluent was subsequently diluted and cultivated, the bactericidal rate of CFU per cm^2 was calculated. Each sample is repeated five times.

3 Results and discussion

3.1 Fabrication and topography characterization of NBs@CSG

To obtain etched surfaces with different topographies, the etching time was controlled, and a series of blade-like nanostructures were prepared, which were named as low-density NBs@CSG, medium-density NBs@CSG, high-density NBs@CSG, and ultra-high-density NBs@CSG (LD-NBs@CSG, MD-NBs@CSG, HD-NBs@CSG and UHD-NBs@CSG; Figure 2). After 1 h of etching, evenly distributed NBs were formed on the CSG surface, and a large number of NBs existed in the form of a single individual (Figure 2a). The NBs fused with each other and gradually formed a blade network structure with the increase of etching time (Figure 2b–d). The statistical results of blade width, length, and density according to SEM are shown in Figure 2e–g. With the increase of etching time to 4 h, the width of the NBs decreases slightly (from 22.21 ± 4.44 to 20.10 ± 4.83 nm), and the blade length increases from 120.95 ± 50.23 to 153.73 ± 66.58 nm. In this process, the blade density increases from 4.0×10^9 to 7.3×10^9 slice cm^{-2}.

3.2 The etching mechanism of CSG

To explore and study the etching process of CSG, the composition of the CSG surface was analyzed. CSG is divided into network formers, network modifiers, and intermediates according to cation types. Network formers are usually composed of $[SiO_4]^{4-}$ units, which usually form a three-dimensional network structure through the interconnection of bridging oxygen. Network modifiers, such as K and Na ions, can interrupt the network and lead to non-bridge oxygen that adjust glass properties. Network intermediates, mainly composed of double-acting cations (Mg, Al), can act as network formers or network modifiers according to environmental changes [55]. EDS is used to analyze various compositions of each surface, and the atomic ratio of network modifiers (Na, K), intermediates (Al, Mg), and network formers (Si) with time is calculated (Figure 3). The results show that the content of Na and K on the surface of CSG decreases rapidly in the condition of thermal-alkali solution, indicating that the network modifiers formed by CSG are dissolved first. Attribute to the cations in this region have a very low binding energy with non-bridge oxygen (Na–O: 94 kJ mol^{-1}, K–O: 54 kJ mol^{-1}),

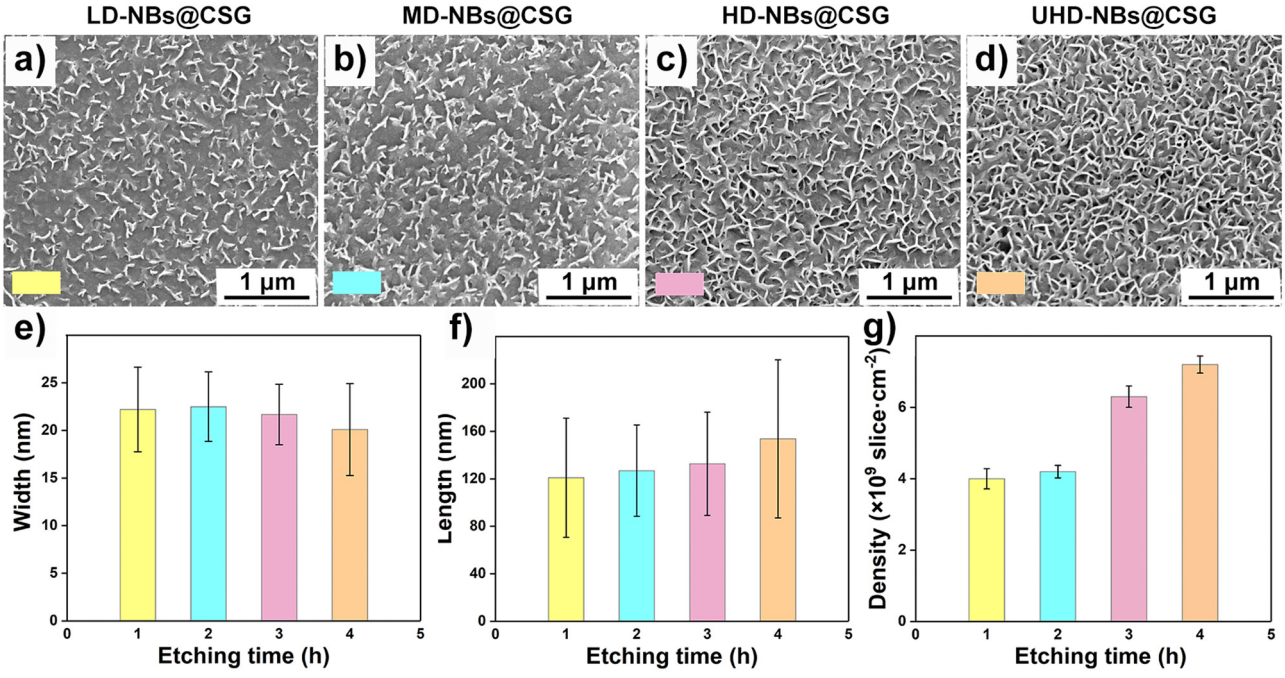

Figure 2: Surface topography and topography statistics of NBs@CSG. SEM images of etched-CSG after etching for different time: (a) 1 h, (b) 2 h, (c) 3 h, and (d) 4 h. Topographic parameters of the NBs: (e) width, (f) length, and (g) density.

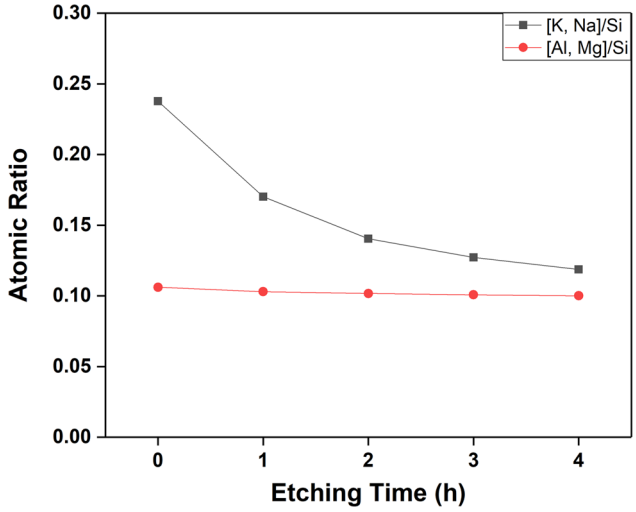

Figure 3: Atomic ratio [cationic/Si] changes with etching time of CSG.

can exchange with hydrogen ions in the water and enter the solution [56]. After Na and K dissolved, the exposed area of network modifiers is more likely to react with water to generate silanol groups, which will further undergo dehydration cross-linking and local network reconstruction to form a single NB (Figure 3a). Then the pores are generated in the network modifier region, allowing water molecules to enter the surface for further etching. Therefore, the growth rate of NBs near the network modifier region is slightly faster. As the reaction continues, the Si–O (bond energy 443 kJ mol^{-1}) in network formers area slowly depolymerize and form to Si–OH (equation (1)) and further form into soluble $Si-O-SiO(OH)_4^-$ (equation (2)) [57]. Near the substrate, $Si-O-SiO(OH)_4^-$ reacts with K^+, Na^+, and Ca^{2+} in solution to form a gel layer, which acts as a barrier, thus reducing the loss rate of Na and K on the CSG surface and delaying the etching rate (Figure 3). Moreover, the gel layer slowly participates in the reconstruction of the NB network [58], which makes the blade length and density continuously increase (Figure 2b–d). With the prolonging of etching time, the width and the height of the NBs were almost negligible, attribute to the high bond energy of Si–O, the low diffusion rate, and blocking effect of the gel layer. The content of Al and Mg decreased slightly during the etching process, also result from the blocking effect of the gel layer and the higher bond energies between the non-bridge oxygen and intermediates cationic. Under the same etching conditions, the size of the NBs obtained on CSG is much larger than that on calcium sodium glass, which may be due to the different content of network modifiers. Calcium sodium glass has a larger number of network modifier regions and therefore a larger number of initial etching sites can be formed during the ion exchange period [59].

$$Si-O-Si + H_2O \leftrightarrow 2Si-OH, \quad (1)$$

$$Si-O-Si(OH)_3 + OH^- \rightarrow Si-O-Si(OH)_4^-. \quad (2)$$

3.3 Density-dependent mechanical bactericidal activity of NBs@CSG

The statistical results of bactericidal experiment were shown in Figure 4a. All of the NB surfaces show a certain

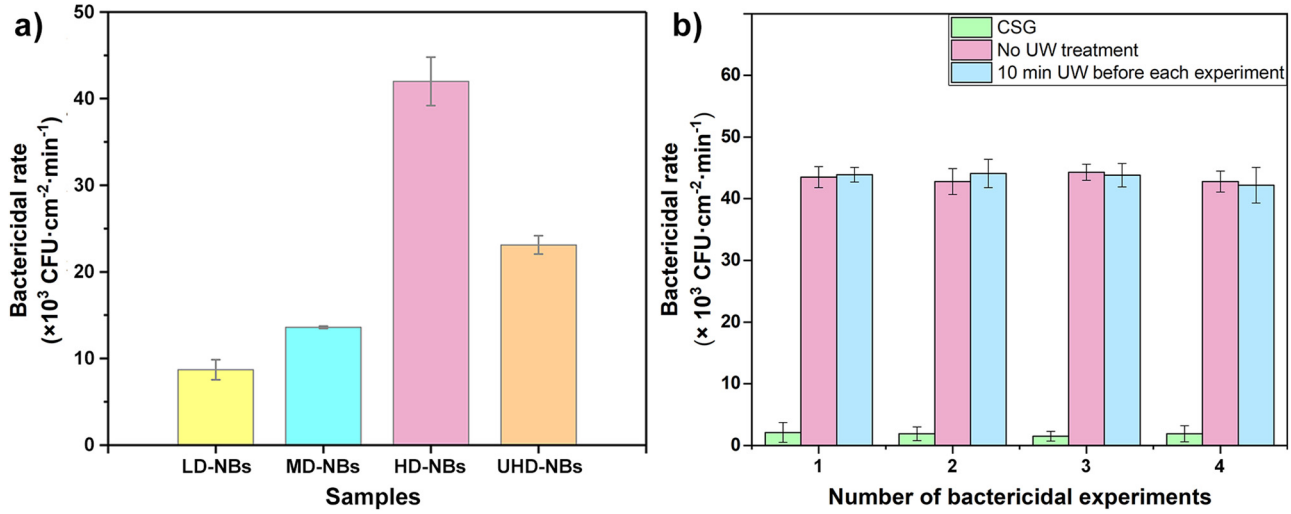

Figure 4: The mechanical bactericidal activity of NBs@CSG. (a) The bactericidal rate against *E. coli* of NBs@CSG with different density. (b) The long-term stability of HD-NBs@CSG bactericidal effect. The 1–4 times consecutive bactericidal experiment statistical results of *E. coli* on HD-NBs@CSG with or without ultrasonic wave treatment. Incubation time: 10 min. The data are expressed as mean ± SD of three replicates.

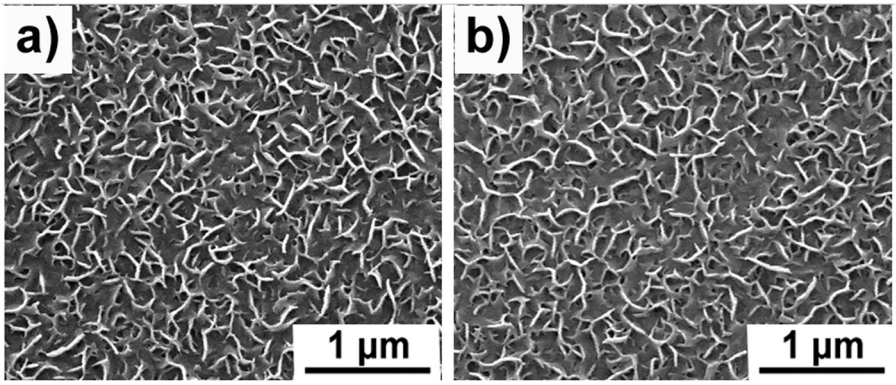

Figure 5: Binding of NBs on CSG substrate surface. The surface topography after ultrasonic cleaning-bactericidal experiment: (a) 2 times and (b) 4 times. The ultrasonic cleaning process: 5 min.

bactericidal activities after 10 min of incubation. And from the LD-NBs to UHD-NBs, the surface bactericidal performance was firstly increased and then decreased. Previous studies have shown that the larger the length of the bactericidal unit tip, the smaller the stress on the bactericidal cell and the poorer the mechano-bactericidal performance. Therefore, the continuous increase in the bactericidal performance of LD-NB to HD-NB samples was mainly caused by the increase of blade density. The increase of blade density can increase the number of the sterilization unit that contact a single cell, resulting in an increased ability to damage the bacterial membrane. The *E. coli* cells (0.5×1–3 μm) are larger in size than NBs. However, the positive correlate promotion effect works only within a certain range. As the blade density further increased, the surface bactericidal activity decreased obviously (Figure 4a). The excessively high blade density may reduce the stress of a single blade on cells due to stress averaging. In addition, the excessively high blade density will also affect the effective sinking of bacterial cells, and reduce the force on cells. Notably, the CSG-NB surface had a lower bactericidal performance than the nanopillar of the same density (black silicon: 4.5×10^5 CFU min^{-1} cm^{-2}, dragonfly wing: 4.5×10^5 CFU min^{-1} cm^{-2}; cicada wing: 2.0×10^5 CFU min^{-1} cm^{-2}) [26], which has a lower tip diameter and can cause higher stress on the bacterial cell [6]. It is worth noting that compared with LD-NBs@CSG, ZnAl lamellar bimetallic hydroxide HD-NBs (ZnAl LDH HD-NBs) prepared in our previous study has similar density and higher width and length (width: 29.32 ± 5.74 nm, length: 880.00 ± 223.62 nm, density: 4.4×10^9 slice cm^{-2}), but the bactericidal rate of ZnAl LDH HD-NBs is higher than that of LD-NBs@CSG ($8.69 \pm 1.16 \times 10^3$ CFU cm^{-2} min^{-1}) [42]. This may be attributed to the low height of LD-NBs@CSG, which could not provide enough altitude difference to provide enough mechanical force on bacterial cells.

To evaluate the long-term bactericidal efficacy of HD-NBs@CSG, a continuous bactericidal experiment was carried out. A complete experiment process was carried out for each test. The results showed that after four times bactericidal experiments, the surface maintained good bactericidal activity and did not significantly decrease (Figure 4), shows a good long-term bactericidal performance. At the same time, the effective combination of NBs and substrate directly affects the surface bactericidal activity, so the ultrasonic pretreatment-bactericidal experimental group is carried out to evaluate the reliability of the performance of the HD-NBs@CSG. An ultrasonic wave cleaning process (100 W, 5 min) was added before each bactericidal experiment. As the result shows in Figure 4b, the bactericidal activity of ultrasonic pretreatment group and the untreated group was not significantly different in four times continuous bactericidal experiments, which shows the bactericidal performance stability. It is well known that the effective combination of nanostructure and substrate directly determines the performance [60]. This is because the NBs combine well with the CSG substrate and the ultrasonic treatment does not affect the nanostructure of the surface (Figure 5).

4 Conclusions

In conclusion, in this study a series of NB structures with gradient densities, similar thickness and height were constructed on the surface of CSG by alkali etching by controlling etching time. The etched NBs@CSG has a mechanical bactericidal activity, and the surface bactericidal activity can be improved by increasing the blade density in a certain range. The NB has an optimal density, which can achieve the highest mechano-bactericidal

performance. Therefore, it is unrealistic to increase the efficiency of mechanical sterilization by increasing the density of bactericidal units. Although our experiments clarified the relationship between CSG–NBs density and mechano-bactericidal performance, the interaction mechanism between other nano units (such as nanopillar and nanocone) and bacteria may be different, so the correlation between these surface nano unit densities and bactericidal performance needs to be further studied. In addition, to solve the long-term application, the good combination between the CSG substrate and the blade was demonstrated by the ultrasonic treatment of HD-NBs sample. Thus, this study provides a simple method and idea for the preparation of fast and efficient bactericidal nanostructures on the surface of CSG in civil aircraft cabin to realize the saving of manual disinfection labor, which is conducive to the further practical application of mechanical bactericidal technology.

Funding information: This study was financially supported by the Science and Technology Planning Project of Sichuan Province (No. 2017RZ0032).

Author contributions: All authors have accepted responsibility for the entire content of this manuscript and approved its submission.

Conflict of interest: The authors state no conflict of interest.

References

[1] Ivanoska-Dacikj A, Stachewicz U. Smart textiles and wearable technologies – opportunities offered in the fight against pandemics in relation to current COVID-19 state. Rev Adv Mater Sci. 2020;59(1):487–505.

[2] Spengler JD, Wilson DG. Air quality in aircraft. Proc Inst Mech Eng Part E J Process Mech Eng. 2003;217(4):323–36.

[3] Schultz M, Evler J, Asadi E, Preis H, Fricke H, Wu CL. Future aircraft turnaround operations considering post-pandemic requirements. J Air Transp Manag. 2020;89:101886.

[4] Yi G, Yuan Y, Li X, Zhang Y. ZnO nanopillar coated surfaces with substrate-dependent superbactericidal property. Small. 2018;14(14):e1703159.

[5] Ivanova EP, Linklater DP, Werner M, Baulin VA, Xu X, Vrancken N, et al. The multi-faceted mechano-bactericidal mechanism of nanostructured surfaces. Proc Natl Acad Sci U S A. 2020;117:12598–605.

[6] Xie Y, Qu X, Li J, Li D, Wei W, Hui D, et al. Ultrafast physical bacterial inactivation and photocatalytic self-cleaning of ZnO nanoarrays for rapid and sustainable bactericidal applications. Sci Total Environ. 2020;738:139714.

[7] He W, Zhang Y, Li J, Gao Y, Luo F, Tan H, et al. A novel surface structure consisting of contact-active antibacterial upper-layer and antifouling sub-layer derived from gemini quaternary ammonium salt polyurethanes. Sci Rep. 2016;6:e32140.

[8] Gholamrezazadeh M, Shakibaie MR, Monirzadeh F, Masoumi S, Hashemizadeh Z. Effect of nano-silver, nano-copper, deconex and benzalkonium chloride on biofilm formation and expression of transcription regulatory quorum sensing gene (rh1r) in drug-resistance *Pseudomonas aeruginosa* burn isolates. Burns. 2018;44(3):700–8.

[9] Jutkina J, Marathe NP, Flach CF, Larsson DGJ. Antibiotics and common antibacterial biocides stimulate horizontal transfer of resistance at low concentrations. Sci Total Environ. 2018;616–617:172–8.

[10] Lin N, Berton P, Moraes C, Rogers RD, Tufenkji N. Nanodarts, nanoblades, and nanospikes: mechano-bactericidal nanostructures and where to find them. Adv Colloid Interface Sci. 2018;252:55–68.

[11] Elbourne A, Crawford RJ, Ivanova EP. Nano-structured antimicrobial surfaces: from nature to synthetic analogues. J Colloid Interface Sci. 2017;508:603–16.

[12] Hasan J, Chatterjee K. Recent advances in engineering topography mediated antibacterial surfaces. Nanoscale. 2015;7(38):15568–75.

[13] Green DW, Lee KK, Watson JA, Kim HY, Yoon KS, Kim EJ, et al. High quality bioreplication of intricate nanostructures from a fragile gecko skin surface with bactericidal properties. Sci Rep. 2017;7:41023.

[14] Cheeseman S, Elbourne A, Kariuki R, Ramarao AV, Zavabeti A, Syed N, et al. Broad-spectrum treatment of bacterial biofilms using magneto-responsive liquid metal particles. J Mater Chem B. 2020;8:10776–87.

[15] Kargar M, Wang J, Nain AS, Behkam B. Controlling bacterial adhesion to surfaces using topographical cues: a study of the interaction of pseudomonas aeruginosa with nanofiber-textured surfaces. Soft Matter. 2012;8(40):10254–9.

[16] Cheng G, Zhang Z, Chen S, Bryers JD, Jiang S. Inhibition of bacterial adhesion and biofilm formation on zwitterionic surfaces. Biomaterials. 2007;28(29):4192–9.

[17] Abee T, Kovács ÁT, Kuipers OP, van der Veen S. Biofilm formation and dispersal in gram-positive bacteria. Curr Opin Biotechnol. 2011;22(2):172–9.

[18] Demssie Dejen K, Amare Zereffa E, Ananda HC, Murthy AM. Synthesis of ZnO and ZnO/PVA nanocomposite using aqueous *Moringa oleifeira* leaf extract template: antibacterial and electrochemical activities. Rev Adv Mater Sci. 2020;59(1):464–76.

[19] Meng J, Zhang P, Wang S. Recent progress in biointerfaces with controlled bacterial adhesion by using chemical and physical methods. Chem – An Asian J. 2014;9(8):2004–16.

[20] Kaplan JB. Biofilm dispersal: mechanisms, clinical implications, and potential therapeutic uses. J Dent Res. 2010;89(3):205–18.

[21] Guilhen C, Forestier C, Balestrino D. Biofilm dispersal: multiple elaborate strategies for dissemination of bacteria with unique properties. Mol Microbiol. 2017;105(2):188–210.

[22] Bielecki M, Patel D, Hinkelbein J, Komorowski M, Kester J, Ebrahim S, et al. Air travel and covid-19 prevention in the pandemic and peri-pandemic period: a narrative review. Travel Med Infect Dis. 2021;39:101915.

[23] Liu M, Wang L, Tong X, Dai J, Li G, Zhang P, et al. Antibacterial polymer nanofiber-coated and high elastin protein-expressing bmscs incorporated polypropylene mesh for accelerating healing of female pelvic floor dysfunction. Nanotechnol Rev. 2020;9:670–82.
[24] Miura T, Shibata T. Antiviral effect of chlorine dioxide against influenza virus and its application for infection control. Open Antimicrob Agents J. 2010;2:71–8.
[25] Ambach F. Antimicrobial and antioxidant activity of silver, gold and silver-gold alloy nanoparticles phytosynthesized using extract of *Opuntia ficus*-indica. Rev Adv Mater Sci. 2019;58(1):313–26.
[26] Ivanova EP, Hasan J, Webb HK, Gervinskas G, Juodkazis S, Truong VK, et al. Bactericidal activity of black silicon. Nat Commun. 2013;4:2838.
[27] Ivanova EP, Hasan J, Webb HK, Truong VK, Watson GS, Watson JA, et al. Natural bactericidal surfaces: mechanical rupture of pseudomonas aeruginosa cells by cicada wings. Small. 2012;8(16):2489–94.
[28] Singh J, Jadhav S, Avasthi S, Sen P. Designing photocatalytic nanostructured antibacterial surfaces: why is black silica better than black silicon? ACS Appl Mater Interfaces. 2020;12(18):20202–13.
[29] Li X. Bactericidal mechanism of nanopatterned surfaces. Phys Chem Chem Phys. 2015;18(2):1311–6.
[30] Bandara CD, Singh S, Afara IO, Wolff A, Tesfamichael T, Ostrikov K, et al. Bactericidal effects of natural nanotopography of dragonfly wing on *Escherichia Coli*. ACS Appl Mater Interfaces. 2017;9(8):6746–60.
[31] Linklater DP, Juodkazis S, Rubanov S, Ivanova EP. Comment on "bactericidal effects of natural nanotopography of dragonfly wing on *Escherichia coli*. ACS Appl Mater Interfaces. 2017;9(35):29387–93.
[32] Linklater DP, Juodkazis S, Ivanova EP. Nanofabrication of mechano-bactericidal surfaces. Nanoscale. 2017;9:16564–85.
[33] Elbourne A, Coyle VE, Truong VK, Sabri YM, Kandjani AE, Bhargava SK, et al. Multi-directional electrodeposited gold nanospikes for antibacterial surface applications. Nanoscale Adv. 2019;1(1):203–12.
[34] Nowlin K, Boseman A, Covell A, LaJeunesse D. Adhesion-dependent rupturing of *Saccharomyces cerevisiae* on biological antimicrobial nanostructured surfaces. J R Soc Interface. 2015;12(102):20140999.
[35] Bhadra CM, Truong VK, Pham VT, Al Kobaisi M, Seniutinas G, Wang JY, et al. Antibacterial titanium nano-patterned arrays inspired by dragonfly wings. Sci Rep. 2015;5:16817.
[36] Pogodin S, Hasan J, Baulin VA, Webb HK, Truong VK, Phong Nguyen TH, et al. Biophysical model of bacterial cell interactions with nanopatterned cicada wing surfaces. Biophys J. 2013;104(4):835–40.
[37] Truong VK, Geeganagamage NM, Baulin VA, Vongsvivut J, Tobin MJ, Luque P, et al. The susceptibility of *Staphylococcus aureus* CIP 65.8 and pseudomonas aeruginosa ATCC 9721 cells to the bactericidal action of nanostructured *Calopteryx haemorrhoidalis* damselfly wing surfaces. Appl Microbiol Biotechnol. 2017;101:4683–90.
[38] Mainwaring DE, Nguyen SH, Webb H, Jakubov T, Tobin M, Lamb RN, et al. The nature of inherent bactericidal activity: insights from the nanotopology of three species of dragonfly. Nanoscale. 2016;8:6527–34.
[39] Watson GS, Green DW, Schwarzkopf L, Li X, Cribb BW, Myhra S, et al. A gecko skin micro/nano structure – a low adhesion, superhydrophobic, anti-wetting, self-cleaning, biocompatible, antibacterial surface. Acta Biomater. 2015;21:109–22.
[40] Linklater DP, De Volder M, Baulin VA, Werner M, Jessl S, Golozar M, et al. High aspect ratio nanostructures kill bacteria via storage and release of mechanical energy. ACS Nano. 2018;12(7):6657–67.
[41] Sengstock C, Lopian M, Motemani Y, Borgmann A, Khare C, Buenconsejo PJ, et al. Structure-related antibacterial activity of a titanium nanostructured surface fabricated by glancing angle sputter deposition. Nanotechnology. 2014;25(19):195101.
[42] Xie Y, Li J, Bu D, Xie X, He X, Wang L, et al. Nepenthes -inspired multifunctional nanoblades with mechanical bactericidal, self-cleaning and insect anti-adhesive characteristics. RSC Adv. 2019;9(48):27904–10.
[43] Watson GS, Green DW, Watson JA, Zhou Z, Li X, Cheung GSP, et al. A simple model for binding and rupture of bacterial cells on nanopillar surfaces. Adv Mater Interfaces. 2019;6(10):1801646.
[44] Diu T, Faruqui N, Sjöström T, Lamarre B, Jenkinson HF, Su B, et al. Cicada-inspired cell-instructive nanopatterned arrays. Sci Rep. 2014;4:7122.
[45] Dickson MN, Liang EI, Rodriguez LA, Vollereaux N, Yee AF. Nanopatterned polymer surfaces with bactericidal properties. Biointerphases. 2015;10(2):e021010.
[46] Fisher LE, Yang Y, Yuen M-F, Zhang W, Nobbs AH, Su B. Bactericidal activity of biomimetic diamond nanocone surfaces. Biointerphases. 2016;11(1):e011014.
[47] Pham VT, Truong VK, Quinn MD, Notley SM, Guo Y, Baulin VA, et al. Graphene induces formation of pores that kill spherical and rod-shaped bacteria. ACS Nano. 2015;9(8):8458–67.
[48] Athauda TJ, Hari P, Ozer RR. Tuning physical and optical properties of ZnO nanowire arrays grown on cotton fibers. ACS Appl Mater Interfaces. 2013;5(13):6237–46.
[49] Wagata H, Ohashi N, Taniguchi T, Subramani AK, Katsumata K, Okada K, et al. Single-step fabrication of ZnO rod arrays on a nonseeded glass substrate by a spin-spray technique at 90°C. Cryst Growth Des. 2010;10(8):3502–7.
[50] Li C, Fang G, Li J, Ai L, Dong B, Zhao X. Effect of seed layer on structural properties of ZnO nanorod arrays grown by vapor-phase transport. J Phys Chem C. 2008;112(4):990–5.
[51] Wu Q, Miao WS, Zhang Y, DuGao D, Hui HJ. Mechanical properties of nanomaterials: a review. Nanotechnol Rev. 2020;9:259–73.
[52] Piret N, Santoro R, Dogot L, Barthélemy B, Peyroux E, Proost J. Influence of glass composition on the kinetics of glass etching and frosting in concentrated HF solutions. J Non Cryst Solids. 2018;499:208–16.

[53] Xie Y, Wei W, Meng F, Qu X, Li J, Wang L, et al. Electric-field assisted growth and mechanical bactericidal performance of zno nanoarrays with gradient morphologies. Nanotechnol Rev. 2019;8(1):315–26.
[54] Jindai K, Nakade K, Masuda K, Sagawa T, Kojima H, Shimizu T, et al. Adhesion and bactericidal properties of nanostructured surfaces dependent on bacterial motility. RSC Adv. 2020;10:5673–80.
[55] Hench LL, Clark DE. Physical chemistry of glass surfaces. J Non Cryst Solids. 1978;28(1):83–105.
[56] Shi C. Corrosion of glasses and expansion mechanism of concrete containing waste glasses as aggregates. J Mater Civ Eng. 2009;21(10):529.
[57] Bunker BC. Molecular mechanisms for corrosion of silica and silicate glasses. J Non Cryst Solids. 1994;179:300–8.
[58] Tournié A, Ricciardi P, Colomban P. Glass corrosion mechanisms: a multiscale analysis. Solid State Ionics. 2008;179(38):2142–54.
[59] Xiong J, Das SN, Kar JP, Choi JH, Myoung JM. A multifunctional nanoporous layer created on glass through a simple alkali corrosion process. J Mater Chem. 2010;20(45):10246–52.
[60] Vlassov S, Oras S, Antsov M, Sosnin I, Polyakov B, Shutka A, et al. Adhesion and mechanical properties of PDMS-based materials probed with AFM: a review. Rev Adv Mater Sci. 2018;56(1):62–78.